

Photoconductance through quantum point contacts: Exact numerical results

Frank A. Maaß

Institutt for Fysikk, Universitetet i Trondheim, Norges Tekniske Høgskole, N-7034 Trondheim, Norway

L. Y. Gorelik

*Department of Applied Physics, Chalmers University of Technology and Göteborg University, S-412 96 Göteborg, Sweden
and B. I. Verkin Institute for Low Temperature Physics and Engineering, 47 Lenin Avenue, 310164 Kharkov, Ukraine*

(Received 3 November 1995; revised manuscript received 5 February 1996)

By utilizing the hybrid recursive Green's function method, we study the exact numerical photoconductance of quantum point contacts and compare it with features obtained in the analytic adiabatic regime. We find that the main features of the photoconductance oscillations are present, but with quantum corrections. These corrections are mainly due to deviations from the semiclassical description of wave functions. Nonadiabatic corrections enhance the photoconductance oscillations. [S0163-1829(96)01524-X]

I. INTRODUCTION

Recently, theoretical interest in the problem of coherent scattering of electrons in microconstrictions of the two-dimensional electron gas (2DEG), due to the presence of an external ac electromagnetic field, has revealed several interesting phenomena.¹⁻³ These results were all based on two assumptions: (i) the strict separation of longitudinal and (quantized) transverse electron motion, and (ii) the semiclassical nature of the longitudinal motion within each transverse mode. Both of these assumptions are justified in an adiabatically varying constriction,⁴ which is believed to be close to the experimental situation.

Quantum corrections to these assumptions must include the following. First, mixing of longitudinal and transverse motion, which can be treated as elastic intermode scattering and allows for momentum transfer between the longitudinal and the transverse direction. Second, quantum corrections to the semiclassical wave function describing longitudinal motion. Both these corrections increase when the geometry of the microconstriction becomes more abrupt and can destroy phenomena arising in the framework of adiabatic ideology. However, the experimental and numerical results show that "adiabatic" phenomena, such as conductance quantization in the point contact, are robust against these corrections. In fact, conductance quantization may even be enhanced by nonadiabatic corrections. As was shown in Ref. 2, the photoconductance of microconstrictions has a much richer structure and could, therefore, be more sensitive to quantum corrections to the adiabatic approximation. The influence of these corrections is what we address in this paper. We shall demonstrate that the corrections can be significant.

Analytic solutions to coherent scattering are difficult to achieve, even in the relatively simple case of the quantum point contact.⁵ The introduction of a time dependent external field increases the complexity of the problem. In the case of a static scattering potential, it has been necessary to complement analytic results with numerical solutions. In the present paper, we describe how to extend an already established numerical method^{6,7} to include the effect of a time dependent electromagnetic field. Subsequently, the method is applied to

the point contact and compared with the analytic results from Ref. 2. The extent to which the results in Ref. 2 can be found in the exact numerical calculations and their deviations will be the focus of our discussion.

II. THEORY

The physical setup that we have in mind is a mesoscopic multiterminal device with ideal leads connecting the scattering area to reservoirs. The main assumptions in the following are that (i) we have a stationary flow and (ii) we can neglect spontaneous emission. That is, electrons enter the scattering region, are scattered, and do not experience any spontaneous emission before they reach the reservoirs (estimates can be found in Ref. 3). We adopt the common assumption of neglecting the electron-electron interaction. Thus, we have a one particle picture. From the above assumptions, two important properties of the resulting scattering probabilities, $T_{\beta\alpha}$, follow. First, $\sum_{\beta} T_{\beta\alpha} = 1$ ensures current conservation. That is, any incoming state, α , is scattered out of the scattering region with a probability of unity (note that β in this description includes all possible outgoing states). Second, $\sum_{\alpha} T_{\beta\alpha} = 1$ ensures that no outgoing state is occupied by more than one particle. That is, *we do not have to worry about the Pauli exclusion principle*. For a further discussion of this point, we refer to Refs. 8-10 and references therein. Usually, it is more convenient to split the general index α/β into one lead index, i/j , and one mode index m/n at the given energy, E . We may then define the total scattering from lead j to lead i as $T_{i,j}(E,E') = \sum_{m,n} T_{(i,m),(j,n)}(E,E')$. We shall further assume that the electromagnetic field is essentially monochromatic (i.e., $\Delta\omega \ll E_F/\hbar, \omega$). The general formula to calculate the current out of reservoir i can therefore be written in the spirit of Landauer and Büttiker¹¹ as (with spin degeneracy),

$$I_i = \frac{2e}{h} \int_0^{\infty} \left[N_i(E) f_{\mu_i}(E) - \sum_j \sum_n T_{i,j}(E) + n\hbar\omega, E) f_{\mu_j}(E) \right] dE, \quad (1)$$

where $f_\mu(E)$ is the Fermi distribution function describing a reservoir with chemical potential μ and $N_i(E)$ is the number of propagating states in lead i at energy E . Note that $T_{i,i}(E+n\hbar\omega, E)$ gives the backscattering in the incident lead i when summed over n . The summation over n is, in principle, over all possible energies $E+n\hbar\omega$. In this paper, we are in the perturbative regime and consider only $n=-1, 0, 1$. In the following discussion, we will consider a two terminal geometry with the reflection symmetry in the longitudinal direction ($x \rightarrow -x$, where x is the longitudinal coordinate). This implies that the current from electrons with energy E incoming from the left (L) is exactly canceled by the same number of electrons incoming from the right (R) at energy E , i.e., $T_{R,L}(E+n\hbar\omega, E) = T_{L,R}(E+n\hbar\omega, E)$ [in this notation; $(i, j) \rightarrow (L, R)$]. Without this symmetry, the current will be induced by the ac field, even in the absence of any applied dc voltage.^{1,12} By noting that $N_L(E) = \sum_n [T_{L,L}(E+n\hbar\omega, E) + T_{R,L}(E+n\hbar\omega, E)]$ and employing the symmetry above, we find that the current out of the left reservoir becomes

$$I_i = \frac{2e}{h} \sum_n \int_0^\infty T_{R,L}(E+n\hbar\omega, E) [f_{\mu_L}(E) f_{\mu_R}(E)] dE. \quad (2)$$

At zero temperature and with a small applied voltage, $eV \ll E_F$, (2) gives the conductance

$$G = \frac{2e^2}{h} \sum_n T_{R,L}(E_F + n\hbar\omega, E_F), \quad (3)$$

where E_F is the Fermi energy. We have assumed $\mu_L > \mu_R$, so that the current goes from left to right. Since the conductance is proportional to the transmission probabilities (by a factor $2e^2/h$), we shall present our results in terms of these rather than the conductance.

There exist several numerical schemes to solve the Schrödinger equation for the case of a static potential. One such numerical method is the recursive Green's function technique.¹³⁻¹⁵ It was originally designed to solve tight-binding Hamiltonians in a channel geometry, but has later been extended to continuous models using a hybrid Hamiltonian.^{6,7} In this description, the transverse direction is expanded in a local set of transverse "eigenfunctions," while the longitudinal, unconfined direction is discretized in a straightforward manner. The advantage of this formulation is that it combines numerical stability (from the Green's function technique) with reasonable computation time (due to use of an optimal size function space for transverse modes). This hybrid technique has been used to study aspects of the quantum point contact and the quite complex problem of antidots in a magnetic field. Since the hybrid model is well described in Refs. 6 and 7, we shall only outline how to formulate the Schrödinger equation in such a way that the recursive Green's function method is applicable. We start by writing down the Schrödinger equation in the effective mass approximation:

$$i\hbar \partial_t \Psi(t) = \hat{H}(t) \Psi(t) = \left[\frac{1}{2m^*} [\vec{p} + e\vec{A}(t)]^2 + V \right] \Psi(t). \quad (4)$$

Here, V is any static potential. We assume the time dependent field to be harmonic, $\vec{A}(t) = \vec{A} \cos(\omega t)$, we neglect the term $(e\vec{A}(t)/2m^*)^2$, and we define

$$\hat{H}_0 \equiv \frac{\vec{p}^2}{2m^*} + V \quad (5)$$

and

$$\hat{A} \equiv \frac{e}{2m^*} (\vec{p} \cdot \vec{A} + \vec{A} \cdot \vec{p}). \quad (6)$$

Going to the Fourier (energy) representation, we find that the Schrödinger equation reads

$$(E - \hat{H}_0) \Psi_E = \hat{A} (\Psi_{E+\hbar\omega} + \Psi_{E-\hbar\omega}), \quad (7)$$

or in matrix form,

$$\hat{S} \vec{\Psi} = 0, \quad (8)$$

where

$$\hat{S} \equiv \begin{pmatrix} \cdot & \cdot & \cdot & \cdot & \cdot \\ \cdot & E + \hbar\omega - \hat{H}_0 & -\hat{A} & 0 & \cdot \\ \cdot & -\hat{A} & E - \hat{H}_0 & -\hat{A} & \cdot \\ \cdot & 0 & -\hat{A} & E - \hbar\omega - \hat{H}_0 & \cdot \\ \cdot & \cdot & \cdot & \cdot & \cdot \end{pmatrix} \quad (9)$$

and

$$\vec{\Psi} \equiv \begin{pmatrix} \cdot \\ \Psi_{E+\hbar\omega} \\ \Psi_E \\ \Psi_{E-\hbar\omega} \\ \cdot \end{pmatrix}. \quad (10)$$

By representing \hat{H}_0 and \hat{A} in the hybrid basis, we are in a position to start calculations. Note that a static magnetic field could be included by redefining \hat{H}_0 and \hat{A} . The retarded Green's function, $\hat{G} \equiv (\hat{S} + i0)^{-1}$, is now of the form

$$\hat{G} = \begin{pmatrix} \cdot & \cdot & \cdot & \cdot & \cdot \\ \cdot & \hat{G}_{E+\hbar\omega, E+\hbar\omega} & \hat{G}_{E+\hbar\omega, E} & \hat{G}_{E+\hbar\omega, E-\hbar\omega} & \cdot \\ \cdot & \hat{G}_{E, E+\hbar\omega} & \hat{G}_{E, E} & \hat{G}_{E, E-\hbar\omega} & \cdot \\ \cdot & \hat{G}_{E-\hbar\omega, E+\hbar\omega} & \hat{G}_{E-\hbar\omega, E} & \hat{G}_{E-\hbar\omega, E-\hbar\omega} & \cdot \\ \cdot & \cdot & \cdot & \cdot & \cdot \end{pmatrix}. \quad (11)$$

The way to proceed is to note that outside the scattering region $\hat{A} = 0$, so that the surface Green's function, $\hat{\Gamma}$, describing the leads is that of the field-free case:

$$\hat{\Gamma} = \begin{pmatrix} \cdot & \cdot & \cdot & \cdot & \cdot \\ \cdot & \hat{\Gamma}_{E+\hbar\omega}^0 & 0 & 0 & \cdot \\ \cdot & 0 & \hat{\Gamma}_E^0 & 0 & \cdot \\ \cdot & 0 & 0 & \hat{\Gamma}_{E-\hbar\omega}^0 & \cdot \\ \cdot & \cdot & \cdot & \cdot & \cdot \end{pmatrix}. \quad (12)$$

The total Green's function is then obtained by successive iteration, using the Dyson equation. The resulting wave function, $\tilde{\Psi}$, as a response to an incoming source, $\tilde{\Psi}_s$, is found via the relation

$$\tilde{\Psi} = -\hat{G}\hat{S}\tilde{\Psi}_s. \quad (13)$$

For details at this point, we refer to the Appendix of Ref. 16. The incoming source, $\tilde{\Psi}_s$, is defined on the interval $(-\infty, -L')$, where the scattering region starts at $-L'$ and ends at L' . In (13) the resulting wave function, $\tilde{\Psi}$, is defined as the remainder of the total wave function, $\tilde{\Psi} + \tilde{\Psi}_s$. From knowledge of the resulting wave function, the scattering probabilities can easily be found. We project out from $\tilde{\Psi}$ the amplitude for a particular outgoing mode β (outside the scattering region), as a result of an incoming mode α in the source term. This amplitude, $\Psi_{\beta;\alpha}$, then gives the scattering probability

$$T_{\beta,\alpha} = \frac{\rho_\alpha}{\rho_\beta} |\Psi_{\beta;\alpha}|^2 = \frac{v_\beta}{v_\alpha} |\Psi_{\beta;\alpha}|^2, \quad (14)$$

where $\rho_{\alpha/\beta}$ is the density of states and $v_{\alpha/\beta}$ is the group velocity of mode α/β .

III. THE POINT CONTACT

A. A review

Since the main goal of this paper is to discuss and extend the results of Ref. 2, it is necessary to recapitulate some of the main findings of Grincwajg *et al.*² On this background, the contribution of the present work will become clear. The basic physics of conductance quantization in point contacts was immediately recognized after its discovery.^{17,18} Quantized motion in the transverse direction of the point contact only allows for a discrete number of modes to propagate through the constriction and each such mode contributes $2e^2/h$ to the conductance. The number of such quanta is determined by the number of transverse states in the middle of the constriction with the eigenenergy below the Fermi energy. One way to view this dynamically is to use the adiabatic picture. An electron enters the point contact region in a given transverse state, n . The change of geometry is then assumed to be so slow that the electron does not scatter into any other transverse state, m . In the longitudinal direction the transverse eigenenergy, $E_n(x)$, will then act as a potential barrier in an effectively one-dimensional scattering problem. In the work by Grincwajg *et al.*² a microwave field, propagating normal to the 2DEG, was polarized in the transverse direction. In their zero field description, the wave functions were of the form

$$\Psi(x,y) \sim \Phi_n(y;x) \exp\left(i \int_0^x k_n(x', E_F) dx'\right), \quad (15)$$

where

$$\left[-\frac{\hbar^2}{2m^*} \frac{\partial^2}{\partial y^2} + V(y;x)\right] \Phi_n(y;x) = E_n(x) \Phi_n(y;x) \quad (16)$$

and

$$k_n(x, E_F) = \sqrt{\frac{E_F - E_n(x)}{\hbar^2/2m^*}}. \quad (17)$$

Here, $V(y;x)$ is the confinement potential which causes a maximum for $E_n(x)$ at $x=0$. They further assumed that any state was either fully transmitted [if $E_n(0) < E_F$] or fully reflected [$E_n(0) > E_F$]. The effect of the ac field was calculated to lowest order in a perturbation expansion, and the transition probabilities were found to be proportional to

$$\left| \int_{-\infty}^{\infty} A_{m,n} \exp\left(i \int_0^x \Delta k(x') dx'\right) dx \right|^2, \quad (18)$$

where

$$\Delta k(x) = \sqrt{\frac{E_F \pm \hbar\omega - E_m(x)}{\hbar^2/2m^*}} - \sqrt{\frac{E_F - E_n(x)}{\hbar^2/2m^*}} \quad (19)$$

and

$$A_{m,n} = -\frac{e\varepsilon}{m^*\omega} \langle m | \hat{p}_y | n \rangle \quad (20)$$

is the matrix element of the interaction between the transverse states Φ_m and Φ_n . Grincwajg *et al.*² assumed a parabolic transverse confinement potential which gave $A_{m,n} \sim \delta_{m\pm 1,n}$, but, in general, transitions may take place between any transverse states with different parity. The evaluation of the integral in Eq. (18) was performed in the stationary phase approximation. In this approximation, it is assumed that most of the contribution to the integral comes from a region near the point, where $\Delta k(x) = 0$. Thus, the point of stationary phase is given by $\hbar\omega = \pm [E_{n\pm 1}(x) - E_n(x)] = \Delta E(x)$. Since $\Delta k(x) = 0$, this also implies that the direction in which the particle moves is not altered during the transition [unless $k_n(x) = 0$].

Grincwajg *et al.*² then varied the minimum width, $W_0 \equiv W(x=0)$, of the constriction, simulating different gate voltages. The effect of varying W_0 is to change the energy of the transverse wave functions, and at zero field the number, $[n_0]$ (where $[\]$ is the integer part), of transverse states below the Fermi energy essentially determines the total transmission. With parabolic transverse confinement potential n_0 is given by

$$n_0 = \frac{E_F}{\Delta E(0)} + \frac{1}{2} = \frac{1}{2} \left(\frac{W_0}{W_0^*} + 1 \right), \quad (21)$$

where W_0^* is the width when the first mode begins to propagate (i.e., $n_0 = 1$). For ‘‘hard walls’’ (i.e., $\Phi_n[y = \pm W(x)/2] = 0$), we have

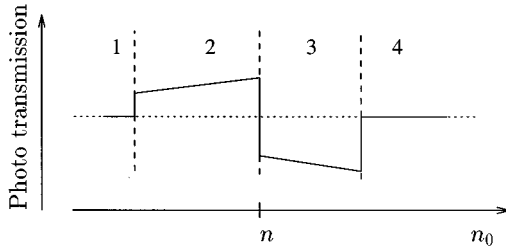


FIG. 1. A typical behavior of the phototransmission near threshold for mode n as found by Grincwajg *et al.* in Ref. 2. Phototransmission is defined as the difference in transmission with a field and without a field. n_0 is the (continuous) number of propagating states at E_F in the narrowest part of the constriction. Both these two quantities have dimensionless units. The figure is divided into four regions, which are explained in the text.

$$n_0 = \frac{k_F W_0}{\pi}. \quad (22)$$

It is also convenient to express the photon energy, $\hbar\omega$, in terms of the Fermi energy. We, therefore, define

$$\Omega \equiv \frac{\hbar\omega}{E_F}. \quad (23)$$

Since transitions from a transmitted state to a reflected state cause reduced transmission (and vice versa), the net result found in Ref. 2 was an oscillatory behavior of the *phototransmission*. We define this quantity as the difference between transmission probabilities with and without field. Figure 1 is a schematic drawing of the typical behavior for the phototransmission near threshold for mode n , as found by Grincwajg *et al.*² In this situation, an electron in mode n can either emit a photon and enter mode $n-1$ or absorb $\hbar\omega$ and enter mode $n+1$. The figure is divided into four regions (labeled 1, 2, 3, and 4), and in the following we shall comment on them successively. In region 1, $E_{n-1}(0) > E_F - \hbar\omega$, and no transition will contribute to the phototransmission. In region 2, $E_{n-1}(0) < E_F - \hbar\omega$ and now the emission to mode $n-1$ gives a positive phototransmission. Since Grincwajg *et al.*² assumed that all zero field transmission probabilities were either zero or one, the phototransmission will make a jump at $E_{n-1}(0) = E_F - \hbar\omega$. At $E_n(0) = E_F$ ($n_0 = n$), mode n becomes transparent and the emission process will not change the phototransmission any more. On the other hand, when $E_n(0) < E_F$ and $E_{n+1}(0) > E_F + \hbar\omega$ (region 3), absorption of $\hbar\omega$ to mode $n+1$ gives a negative phototransmission. At $E_n(0) = E_F$ ($n_0 = n$), they therefore found a jump from positive to negative phototransmission. As W_0 increases further, $E_{n+1}(0) < E_F + \hbar\omega$ (region 4 in Fig. 1) and the absorption process no longer changes the total transmission and the phototransmission goes to zero again. As W_0 increases, the energy difference, $\Delta E(x)$ [as well as $E_n(x)$], between the transverse levels decreases, and when $\Delta E(0) < \hbar\omega$, there are no more stationary points. Grincwajg *et al.*² found that the effect of the field should, therefore, vanish at this point. This means that there is a cutoff value for the oscillations at

$$n_0 = \frac{E_F}{\hbar\omega} + \frac{1}{2} = \frac{1}{\Omega} + \frac{1}{2} \quad (24)$$

for parabolic confinement. This line of argument is more complicated for hard wall confinement, since transitions are not restricted to the nearest modes ($n \pm 1$). If we consider the value for n_0 where transitions to the nearest modes should vanish, then this is given by

$$n_0 = \frac{1}{\Omega} (1 + \sqrt{1 + \Omega}). \quad (25)$$

Note that cutoff will occur only if an increase of the gate voltage leads to a decrease in $\Delta E(0)$.

B. Exact numerical results

1. Adiabatic regime

So far, we have only reviewed some of the main results of Ref. 2 and we shall now turn to the exact calculations. In our numerical calculations, we have considered two different shapes,

$$\frac{W_1(x)}{W_\infty} = \begin{cases} \frac{W_0}{(W_\infty - W_0)\cos^4(\pi x/2L) + W_0}, & |x| \leq L \\ 1, & |x| > L, \end{cases} \quad (26)$$

$$\frac{W_2(x)}{W_\infty} = \begin{cases} 1 - \left(1 - \frac{W_0}{W_\infty}\right) \cos^2\left[\frac{\pi}{2}\left(\frac{x}{L}\right)^2\right], & |x| \leq L \\ 1, & |x| > L. \end{cases} \quad (27)$$

For parabolic confinement potentials, these are defined by the requirement that $y = \pm W_i(x)$ are equipotential lines, and at $n_0 = 1$, we have chosen $W_0/W_\infty = 1/23$. The *parabolic* confinement potentials are, therefore, given as

$$V_i(y;x) = E_F \frac{y^2}{W_i(x)^2}, \quad (28)$$

while the *hard wall* confinement potentials are given as

$$V_i(y;x) = \begin{cases} 0, & |y| < W_i(x)/2 \\ \infty, & |y| \geq W_i(x)/2. \end{cases} \quad (29)$$

Our choice of confinement potentials has the following two benefits. First, all overlap integrals needed to build up our Hamiltonian in the hybrid representation can be calculated analytically. Second, these two choices represent two extreme cases, one with ‘‘soft’’ confinement and one with ‘‘hard’’ confinement. This should reveal features dependent on the specific choice of confinement potential. In this context, the difference between equidistant and nonequidistant energy levels is most important. In order to simulate different gate voltages, we open the point contacts by increasing the values of W_∞ and W_0 by the same amount. As far as the authors know, it is an open question what really happens to the point contact potential when the gate voltage is altered. The shapes are indicated in the inset of Fig. 2, which shows the zero field transmissions for parabolic confinement. The shape defined by Eq. (27) gives the most pronounced quantization of transmission. In our calculations, we use a

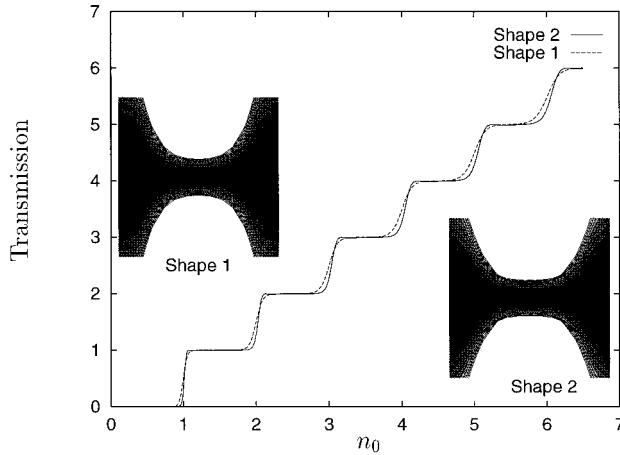


FIG. 2. Zero field transmissions for two different shapes of the point contact potential. The parabolic confinement potentials are indicated by the insets. Shape 1 corresponds to equipotential lines given by Eq. (26) and shape 2 by Eq. (27).

smoothly varying field in order to avoid any interference due to abrupt switching. The strength of the field is varied as $\mathcal{E} \sim 1 - \sin^8(\pi x/2L')$ (when $|x| < L'$), and in the adiabatic regime we use $L' = 2L$. One interesting feature of the present results is the values of the electric field. With the Fermi wave number $k_F = 1.3 \times 10^8 \text{ m}^{-1}$, W_0 in the range of 0 to $0.3 \mu\text{m}$, and an effective mass $m^* = 0.067 \times m_e$, we obtained our results with fields $\mathcal{E} \approx 150 \text{ V/cm}$. This is in good agreement with what was used in Ref. 2, although one has to keep in mind that a different shape [$W(x) = W_0 \exp(x^2/2L^2)$] of the constriction was used. Thus, it should be possible to observe phototransmission with fields of the order 100 V/cm . Figure 3(a) shows the phototransmission for the parabolic confinement potential and $\Omega = 0.35$ (i.e., $\hbar\omega = 0.35E_F$), while Fig. 3(b) shows the phototransmission for hard walls and $\Omega = 0.5$. The first case was considered in Ref. 2. The corresponding cutoff values for n_0 are indicated by vertical lines in the figures.

In Ref. 2 it was assumed that the zero field transmission probabilities were either zero or one. This resulted in steplike oscillations. As can be seen from the figures, the finite transition region between plateaus modifies this picture. The steplike behavior of the oscillations has become more rounded, but it is recognizable in Fig. 3 for the shape given by (27) and with $n_0 < 3$. If we increase the length of the constriction, the steplike behavior becomes clearer. In Fig. 4 we show the results of the same calculation as in Fig. 3(a) (shape 2), but with a constriction twice as long (i.e., a total length of $0.6 \mu\text{m}$). It is clear that the point contact that shows better quantization of zero field transmission also gives the most pronounced steplike behavior of the phototransmission. Notice that there is no steplike structure for $n_0 < 1$, in contrast to the prediction in Ref. 18. This confirms that the main contribution to transitions is from points of stationary phase and not from classical turning points.¹⁹ Perhaps the most prominent feature of the oscillations are the sharp peaks followed by sharp dips near threshold. Although the steplike character is modified, we see that the amplitude of the oscillations increases until cutoff is reached. This increase agrees

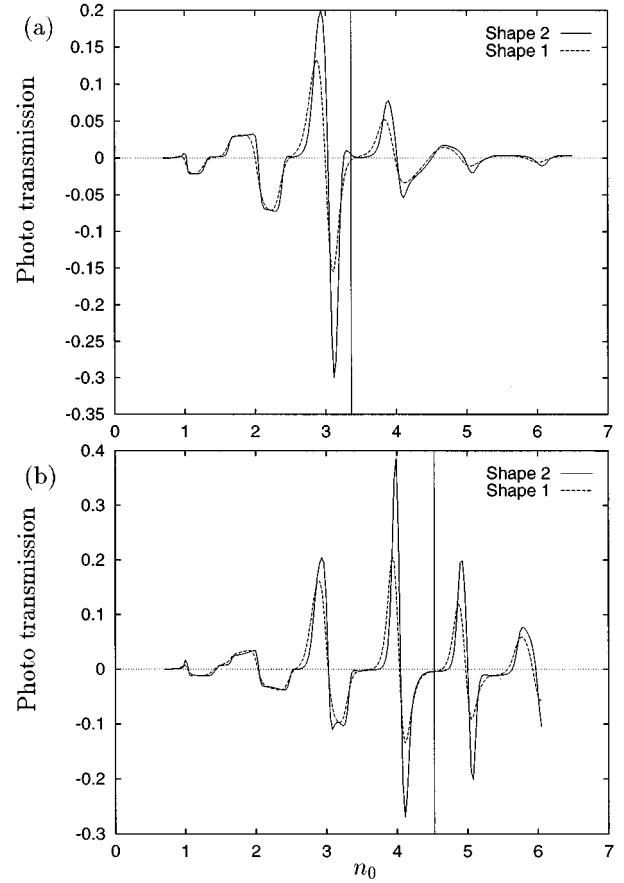


FIG. 3. Phototransmissions as a function of n_0 . The solid lines display transmissions for shape 2 and the dashed lines for shape 1. The vertical lines indicate the points beyond which the phototransmissions should be zero, according to adiabatic theory. (a) Phototransmission for $\hbar\omega = 0.35 \times E_F$ and parabolic confinement potential. The strength of the ac field is $\mathcal{E} = 150 \text{ V/cm}$. (b) Phototransmission for $\hbar\omega = 0.5 \times E_F$ and hard wall confinement potential. The strength of the ac field is $\mathcal{E} = 200 \text{ V/cm}$.

with the analytic result.² The cutoff is not a sharp feature, but the amplitudes of the oscillations are damped after the cutoff value has been reached. For hard wall confinement the cutoff given by (25) is not so prominent as for the parabolic case, but this should be expected from our remarks before Eq. (25). In the following discussion we therefore consider parabolic confinement, which seems to be the most transparent situation.

Let us first consider the absorption process. The transition amplitude from one mode to another is proportional to the overlap integral in Eq. (18) (in the perturbative regime), which includes an evaluation of the integral

$$\int_{-\infty}^{\infty} \exp\left(i \int_0^x \Delta k(x') dx'\right) dx, \quad (30)$$

with

$$\Delta k(x) = \sqrt{\frac{E_F + \hbar\omega - E_{n+1}(x)}{\hbar^2/2m^*}} - \sqrt{\frac{E_F - E_n(x)}{\hbar^2/2m^*}}. \quad (31)$$

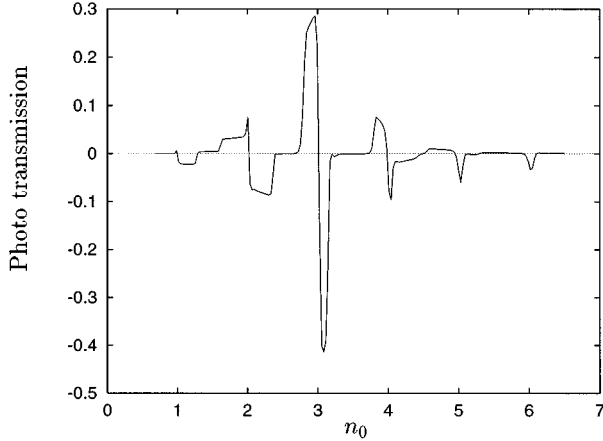


FIG. 4. Phototransmission for parabolic confinement potential. The calculations are performed under the same conditions as in Fig. 2(a) (shape 2), but with a length which is twice as long (i.e., $L \rightarrow 2L$).

At stationary points, $\Delta k(x) = 0$, and we get the main contribution to the overlap integral near this point. When $\Delta E(x=0) < \hbar\omega$, there are no stationary points, but near threshold $E_F \approx E_n(0)$ and we can approximate (31) as

$$\Delta k(x) \approx \Delta k_0 = \sqrt{\frac{\hbar\omega\Delta - E(0)}{\hbar^2/2m^*}}. \quad (32)$$

In order to have a reasonable transition amplitude, we impose the condition that $\Delta k_0 l < \pi$, where l is the typical length of the inner region in the point contact. Substituting $\Delta E(0)(n_0 - 1/2) = E_F$ and $\hbar\omega = \Omega E_F$, this results in the condition that

$$n_0 < \frac{1}{\Omega - \left(\frac{\pi}{kFl}\right)^2} + \frac{1}{2} \equiv \frac{1}{\Omega'} + \frac{1}{2}. \quad (33)$$

The above argument was for an absorption process, and now [in contrast to the situation when $\Delta E(0) > \hbar\omega$] the effect of absorption is to enhance transmission. This follows since mode $n+1$ is more transparent than mode n [$E_F \approx E_n(0)$, while $E_F + \hbar\omega > E_{n+1}(0)$]. From (33), we see that damping is more efficient for long constrictions. For an emission process, the situation is slightly different. Following the same argumentation as above, we find that $\Delta k(x)$ becomes imaginary [since $E_F - \hbar\omega < E_{n-1}(0)$ when $E_F \approx E_n(0)$], and that the overlap integral (30) is $\sim [1 - \exp(-\kappa l)]/\kappa$, where $\kappa = \Delta k_0$. In this case, transmission will decrease, but here the effect is larger for long constrictions. We can notice these two effects by comparing Figs. 3(a) and 4. While the relative height of the peaks decreases when $L \rightarrow 2L$, the amplitude of the dips increases. We would like to stress that the above results are only approximate and do not take into account any virtual processes which gives contributions to $T_{\beta,\alpha}(E_F, E_F)$ in the same order ($\sim \mathcal{E}^2$). From a perturbation expansion of (13), we find

$$\begin{aligned} |\Psi_{E_F, E_F}(x)|^2 &= |\Psi_{E_F}^0(x)|^2 \\ &+ 2\text{Re}[\Psi_{E_F}^0(x)^* \langle x | \hat{G}^0(E_F) \hat{A} \\ &\times \hat{G}^0(E_F \pm \hbar\omega) \hat{A} \hat{G}^0(E_F) \hat{S} | \Psi_s \rangle]. \quad (34) \end{aligned}$$

Clearly, the correction term in (34) is rather difficult to evaluate, especially since it is phase sensitive. On the other hand, we know that this correction must compensate any transition to $E_F \pm \hbar\omega$, and the correction amplitude is essentially given by overlap integrals such as (30).

It is interesting that the cutoff leads to a damping of the oscillations so that they eventually die out. In an experiment, one would therefore obtain some information about what happens with the self-consistent potential near the point contact. If altering the gate voltage merely means to change a local offset potential near the point contact, no damping of the oscillations will be seen. It should, therefore, be possible to see to what extent the gate voltage influences the width of the constriction.

2. Nonadiabatic regime

As mentioned in the previous subsection, the analytic work in Ref. 2 was based on the adiabatic approximation. The adiabatic approximation assumes that the variation of geometry is so slow that it does not cause intermode scattering. That is, if an electron enters the scattering region in a given mode, it will continue within this mode throughout the scattering region (at zero ac field). The scattering problem then becomes one-dimensional with a scattering potential given by the x -dependent eigenenergy, $E_n(x)$, of that particular mode. In Ref. 6, the effect of strong nonadiabaticity on transport through a quantum point contact in zero ac field was studied. It was found that the effect of mode mixing was to enhance the quantization of the conductance. This was found to be caused by the existence of a longitudinal persistence length, $l \sim W_0$, the origin of which is the uncertainty relation, $\Delta x \Delta k \sim 1$. The net effect was that the exact wave function experiences a smoother constriction than the one defined by geometry alone.

One would expect that some nonadiabatic effects will also show up in the phototransmission of a point contact. Since the main contribution to the overlap integral (which determines the transition probability) comes from the region around the stationary point, the transition probability is strongly dependent on how long the region of (approximately) stationary phase is. In essence, this means that the amplitudes of oscillations for the phototransmission becomes smaller the more rapidly the geometry varies. Therefore, one can expect that calculations of phototransmission using the adiabatic approximation would give a smaller amplitude of oscillations than the exact calculations. Figure 5 shows an example. The shape of the point contact is indicated in the inset of the figure. Here, we have used $\Omega = 0.35$ and hard wall boundaries. The calculations seem to confirm our picture. The strength of the ac field is 100 V/cm. For parabolic confinement, this effect is harder to see. This is mainly due to tunneling through the constriction walls, which washes out the quantization of transmission. However, enhancement of the exact calculated phototransmission with respect to the adiabatic approximation can be seen already near the adia-

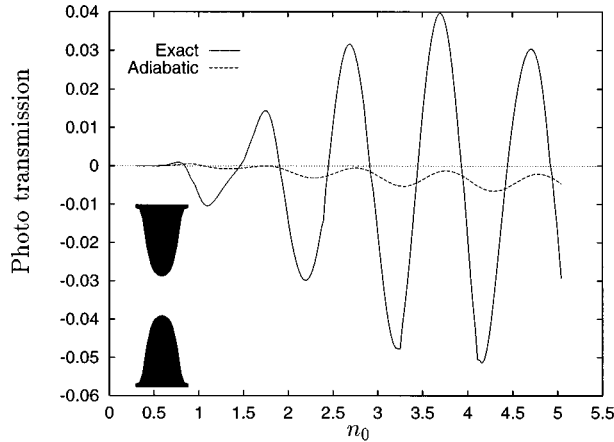


FIG. 5. Phototransmissions for a hard wall confinement potential in the nonadiabatic regime. The solid line displays phototransmission for the exact calculations, while the dashed line indicates phototransmission using the adiabatic approximation. The shape of the point contact is shape 1 [Eq. (26)] and is indicated in the inset. The strength of the ac field is $\mathcal{E}=100$ V/cm.

batic regime as in the previous subsection. Figure 6 shows a comparison between exact and adiabatic calculations under the same conditions as for Fig. 3(a) with shape 2.

C. Comments on two experiments

In two experiments by Wyss *et al.*²⁰ and Janssen *et al.*,²¹ the effect of far-infrared radiation on transport through quantum point contacts was measured. In the experiment by Janssen *et al.*,²¹ unpolarized radiation was used and this also seems to be the case for the experiment by Wyss *et al.*,²⁰ but is not explicitly stated. Thus, our calculations cannot completely describe these experiments. Wyss *et al.* were inspired by the work of Feng and Hu¹⁹ and were looking for steplike oscillations of the photoconductance. Instead, they found oscillations without any steplike character. This was interpreted as a result of bolometric effects (heating of the 2DEG) rather than photon-assisted transport. Janssen *et al.*²¹ discussed this point and the conclusion was that heating effects are too small and cannot be responsible for the observed photoconductance. From our Figs. 2 and 3, one can see that the quantization of transmission must be very good in order to observe the steplike behavior of photoconductance. By looking at the zero field conductance curves from these two experiments, it is therefore no surprise that a steplike behav-

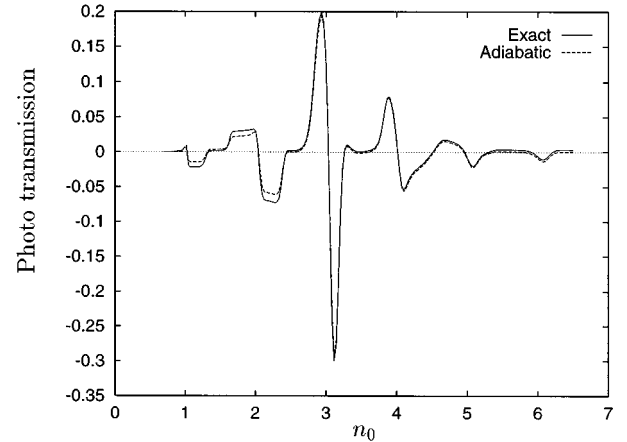


FIG. 6. Phototransmissions for parabolic confinement potential in the adiabatic regime. The solid line displays phototransmission for the exact calculations, while the dashed line indicates phototransmission using the adiabatic approximation (i.e., without elastic intermode scattering).

ior is not present. It is interesting to note that in Ref. 21 photon-induced voltage was observed at zero source/drain current. This indicates that the point contact configuration used was not completely symmetric. This asymmetry could be due to impurity potentials in the vicinity of the constriction region. To conclude this section, we summarize the experimental condition necessary to observe the effects described in this paper. The point contact potential should be symmetric. This may be a limitation if one wishes to study the steplike oscillations, which requires a rather long contact region without any severe impurity potential within its neighborhood. In the adiabatic regime, we used a typical length of 150 nm in the inner region of the point contact. The electric field should be of the order 100 V/cm within the 2DEG, and we remind the reader that our calculations were done with a linear polarized field in the transverse direction. For further details of experimental realization, we refer to Refs. 20 and 21.

ACKNOWLEDGMENTS

F.A.M. acknowledges financial support from the Nordic Research Academy (NorFA) and the hospitality of the Department of Physics at Chalmers University. We gratefully acknowledge stimulating discussions with M. Jonson, R. I. Shekter, and E. H. Hauge.

¹Frank Hekking and Yu. V. Nazarov, Phys. Rev. B **44**, 11 506 (1991).

²A. Grincwajg, L. Y. Gorelik, V. Z. Kleiner, and R. I. Shekter, Phys. Rev. B **52**, 12 168 (1995).

³L. Y. Gorelik, A. Grincwajg, V. Z. Kleiner, R. I. Shekter, and M. Jonson, Phys. Rev. Lett. **73**, 2260 (1994).

⁴L. I. Glazman, G. B. Lesovik, D. E. Khmel'nitskii, and R. I. Shekter, Pis'ma Zh. Éksp. Teor. Fiz. **48**, 218 (1988) [JETP Lett. **48**, 238 (1988)].

⁵A. Yacoby and Y. Imry, Phys. Rev. B **41**, 5341 (1990).

⁶Frank A. Maaß, I. V. Zozulenko, and E. H. Hauge, Phys. Rev. B **50**, 17 320 (1994).

⁷I. V. Zozulenko, Frank A. Maaß, and E. H. Hauge, Phys. Rev. B **53**, 7975 (1996); **53**, 7987 (1996).

⁸A. M. Kríman, N. C. Kluksdahl, and D. K. Ferry, Phys. Rev. B **36**, 5953 (1987).

⁹Supriyo Datta, Phys. Rev. B **45**, 1347 (1992).

¹⁰L. Bönig and K. Schönhammer, Phys. Rev. B **47**, 9203 (1993).

- ¹¹R. Landauer, IBM J. Res. Dev. **1**, 223 (1957); M. Büttiker, Phys. Rev. Lett. **57**, 1761 (1986).
- ¹²L. Fedichkin, V. Ryzhii, and V. V'yurkov, J. Phys. Condens. Matter **5**, 6091 (1993).
- ¹³D. S. Fischer and P. A. Lee, Phys. Rev. B **23**, 6851 (1981).
- ¹⁴A. MacKinnon, Z. Phys. B **59**, 385 (1985).
- ¹⁵F. Sols, M. Macicci, U. Ravaioli, and K. Hess, J. Appl. Phys. **66**, 3892 (1989).
- ¹⁶J. A. Støvneng and E. H. Hauge, Phys. Rev. B **44**, 13 582 (1991).
- ¹⁷B. J. van Wees, H. van Houten, C. W. J. Beenaker J. G. Williamson, L. P. Kouwenhoven, D. van der Marel, and C. T. Foxon, Phys. Rev. Lett. **60**, 848 (1988).
- ¹⁸D. A. Wharam, T. J. Thornton, R. Newbury, M. Pepper H. Ahmed, J. E. F. Frost, D. G. Hasko, D. C. Peacock, D. A. Ritchie, and G. A. C. Jones, J. Phys. C **21**, L209 (1988).
- ¹⁹Shechao Feng and Qing Hu, Phys. Rev. B **48**, 5354 (1993).
- ²⁰Rolf A. Wyss, C. C. Eugster, J. A. del Alamo, and Qing Hu, Appl. Phys. Lett. **63**, 1522 (1993).
- ²¹T. J. B. M. Janssen, J. C. Maan, J. Singleton, N. K. Patel, M. Pepper, J. E. F. Frost, D. A. Ritchie, and G. A. C. Jones, J. Phys. Condens. Matter **6**, L163 (1994).